A Novel Step-Up Multiinput DC–DC Converter for Hybrid Electric Vehicles Application

Rouzbeh Reza Ahrabi, Hossein Ardi, Mahdi Elmi, and Ali Ajami

***Abstract*—In this paper, a multiinput dc–dc converter is proposed and studied for hybrid electric vehicles. Compared to conventional works, the output gain is enhanced. Fuel cell (FC), photovoltaic panel, and energy storage system are the input sources for the proposed converter. The FC is considered as the main power supply, and roof-top PV is employed to charge the battery, increase the efficiency, and reduce fuel economy. The converter has the capability of providing the demanded power by load in absence of one or two resources. Moreover, the power management strategy is described and applied in a control method. A prototype of the converter is also implemented and tested to verify the analysis.**

***Index Terms*—Hybrid electric vehicle (HEV), multiinput converter, power management.**

I. Introduction

GLOBAL warming and lack of fossil fuels are the main drawbacks of vehicles powered by oil or diesel. In order to overcome the aforementioned problems and regarding the potential of clean energies in producing electricity, car designers have shown interest in hybrid electric vehicles (HEVs) and plug-in hybrid electric vehicles. The overall structure of HEV powered by renewable resources is depicted in Fig. 1. Electric vehicles (EVs) have also been studied. EVs rely on energy stored in energy storage system (ESS) [1]. Limited driving range and long battery charging time are their main drawbacks. However, by using a bidirectional on/off board charger, they could have the V2G capability. Solar-assisted EVs have also been studied. Required location and size of PV panels have made them impractical at present [2]. Employing fuel cell as the main power source of HEVs is the result of many years of research and development on HEVs. Pure water and heat are the only emissions of fuel cells. Furthermore, FCs have other advantages like high density output current ability, clean electricity generation, and high-efficiency operation [3]. However, high cost and poor transient performance are the main problems of FCs. It is important to note that vehicles mainly powered by FCs are hybridized by ESS. The main advantages of hybridizing are enhancing fuel economy, providing a more flexible operating strategy, overcoming fuel cell cold start and transient problems, and reducing the cost per unit power [4].

In the literature, few numbers of researches have been reported on EVs' and HEVs' electronic interfaces. In [5], Miaosen has studied employing a Z-source inverter for EV vehicles. Boosting input voltage in one stage is its advantage, while high voltage and current stress and complex control method are the main drawbacks of the presented converter. Another approach was done in [6]. The system was powered by FC and a battery unit. V2G is one of the advantages of the proposed converter. However, the great number of power switches could reduce the reliability and increase the cost. In [7], a multiinput dc–dc boost converter for hybrid PV/FC/Battery is proposed, but the proposed converter cannot work properly because the battery can be only discharged by PV and only charged by FC. In [8], a two-input dc–dc converter is proposed to interface two power sources with a dc bus or load. The converter has high efficiency due to achieving turn-on zero voltage switching of all switches. However, it lacks a bidirectional port. Hence, in applications in need of ESS, it cannot be used. A compact two-input converter is proposed for standalone PV systems in [9]. Moreover, high-voltage gain of the converter makes the converter suitable for low-input voltage applications. However, the high number of semiconductors and passive elements reduce the efficiency.

Control method preset in the vehicle's controller should control the power flow between renewable resources, battery unit, and electrical motor. Optimal utilization of power resources, providing demand power permanently, operating fuel cell, and PV panel in their optimum region are the main duties of control scheme. Some converters have been proposed recently for PVs systems [10]–[12], but the required converter for HEV applications should extract power from PV and FC. Besides, in order to supply back-up power from the battery, a bidirectional port is needed to charge and discharge the battery according to discrepancy between generated power and demanded energy [13], [14]. A multiinput converter can provide power to the load from different energy sources simultaneously or individually.

In the literature, several attempts have been done to get the task done [15]–[19]. An attempt has been done in [20], in which an intelligent optimal power management was introduced. The scheme has three main advances including control of temperature fan, fuzzy hydrogen control, and adaptive current–voltage fast-charging control. In [21], a two-layer energy management has been studied. Minimizing hydrogen consumption is the objective of this study.

Due to the fact that initial cost of PVs is high and in order to increase the extracted power from the PV panels, MPPT

Manuscript received March 7, 2015; revised September 1, 2015 and December 3, 2015; accepted February 17, 2016. Date of publication June 24, 2016; date of current version February 2, 2017. Recommended for publication by Associate Editor S. Williamson.

The authors are with the Electrical Engineering Department, Azarbaijan Shahid Madani University, Tabriz 37200-000, Iran (e-mail: ahrabi@azaruniv.edu; ardi@azaruniv.edu; m.elmi@azaruniv.edu; ajami@azaruniv.edu).

Color versions of one or more of the figures in this paper are available online at http://ieeexplore.ieee.org

Digital Object Identifier 10.1109/TPEL.2016.2585044

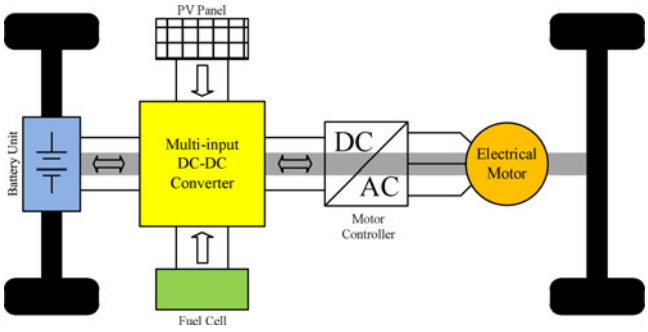

Fig. 1. General structure of the multipowered HEV.

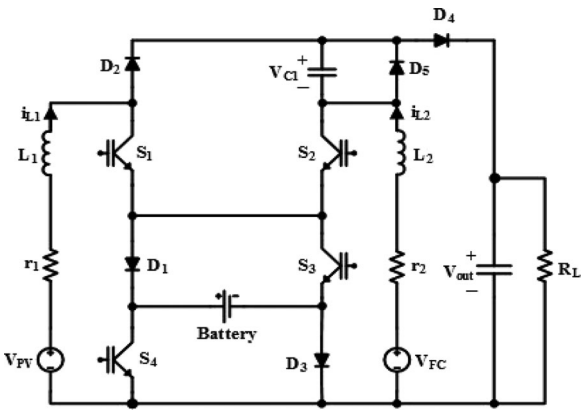

Fig. 2. Three-input dc–dc boost converter.

algorithm has to be utilized. In [22], a general comparison is made between different MPPT techniques with respect to tracking factor, dynamic response, PV voltage ripple, and use of sensors. The other way to improve the efficiency is to enhance the efficiency of the electric components [23].

In this study, a novel three-input dc–dc converter is proposed to merge a PV, a fuel cell, and a battery and connect them to the grid. Furthermore, dc gain is enhanced in respect of conventional converters. Meanwhile, MPPT can be obtained for PV. The battery can be charged and discharged in order to achieve power management. In the following two sections, the proposed structure is studied and different operation modes are discussed. In Section IV, the converter is modeled and linearized to control the converter. Principles of power management and MPPT algorithm are explained in Section V. Additional advantages and useful features of the presented converter and adapting it to HEVs are discussed in Section VI. In Section VII, practical results of the proposed converter are given. Finally, Section VIII concludes the whole paper.

II. Proposed Converter Topology

The structure of the proposed three-input dc–dc boost converter is depicted in Fig. 2. The converter is formed of two conventional boost converters, substituting extra capacitor in one of the converters, and a battery to store the energy. Characteristic of the converter is suitable for hybrid systems. In this paper, behavior of the converter in terms of managing the sources is analyzed in power management and control part. Then, $v_{\rm PV}$ and v_{FC} are two independent power sources that output is based on characteristic of them. L_1 and L_2 are the inductances of input filters of PV panel and fuel cell. Using L_1 and L_2 as in series with input sources change PV and FC modules to current sources. r_1 and r_2 are $v_{\rm PV}$'S and v_{FC}'S equivalent resistance, respectively. $R_{\rm Load}$ is the equivalent resistance of loads connected to the dc bus. S_1, S_2, S_3, and S_4 are power switches. Diodes D_1, D_2, D_3, and D_4 are used to establish modes, which will be described. Capacitor C_1 is used to increase output gain and output capacitor C_o is performed as an output voltage filter. System is operating in continuous-conduct mode to produce smooth current with least possible amount of current ripple.

III. Operation Modes

In this section, principles of the proposed converter are discussed. Operation of the converter is divided into three states: 1) The load is supplied by PV and FC and battery is not used. 2) The load is supplied by PV, FC, and battery, in this state, battery is in discharging mode. 3) The load is supplied by PV and FC and battery is in charging mode.

A. First Operation State (the Load is Supplied by PV and FC While Battery is Not Used)

In this state, as it is illustrated in Fig. 3, there are three operation modes. During this state, the system is operating without battery charging or discharging. Therefore, there are two paths for current to flow (through S_3 and D_3 or D_1 and S_4). In this paper, S_3 and D_3 is considered as common path. However, D_1 and S_4 could be chosen as an alternative path. During this state, switch S_3 is permanently ON and switch S_4 is OFF.

Mode 1: $(0 < t < d_1T)$*:* In this interval, switches S_1, S_2, S_3, and diode D_3 are turned ON. Inductors L_1 and L_2 are charged via power sources $v_{\rm PV}$ and v_{FC}, respectively [see Fig. 3(a)].

Mode 2: $(d_1T < t < d_2T)$*:* In this interval, switch S_1 is turned OFF and D_2 is turned ON and S_2, S_3, and D_3 are still ON. Inductor L_2 is still charged and inductor L_1 is being discharged via $V_{\rm PC} - V_{FC}$[see Fig. 3(b)].

Mode 3: $(d_2T < t < T)$*:* In this interval, S_1 is turned ON and S_2 is turned OFF and S_3 and D_3 are still ON. Inductor L_1 is charged with $v_{\rm PV}$ and inductor L_2 is discharged via $V_{\rm PV} + V_{C1} - V_o$[see Fig. 3(c)].

By applying the voltage–second balance low over the inductors L_1 and L_2, voltage of capacitor C_1 and output voltage can be obtained as follows:

$$L_1 : d_1\left[V_{\rm PV} - r_1 i_{L_1}\right] + (d_2 - d_1)\left[V_{\rm PV} - r_1 i_{L_1} - V_{C_1}\right] + (1 - d_2)\left[V_{\rm PV} - r_1 i_{L_1}\right] = 0 \quad (1)$$

$$V_{C_1} = \frac{V_{\rm PV} - r_1 i_{L_1}}{d_2 - d_1} \quad (2)$$

$$L_2 : d_2\left[V_{FC} - r_2 i_{L_2}\right] + (1 - d_2)\left[V_{FC} + V_{C_1} - r_2 i_{L_2} - V_o\right] = 0 \quad (3)$$

$$V_o = \frac{(d_2 - d_1)\left(V_{FC} - r_2 i_{L_2}\right) + (1 - d_2)\left(V_{FC} - r_1 i_{L_1}\right)}{(1 - d_2)(d_2 - d_1)}. \quad (4)$$

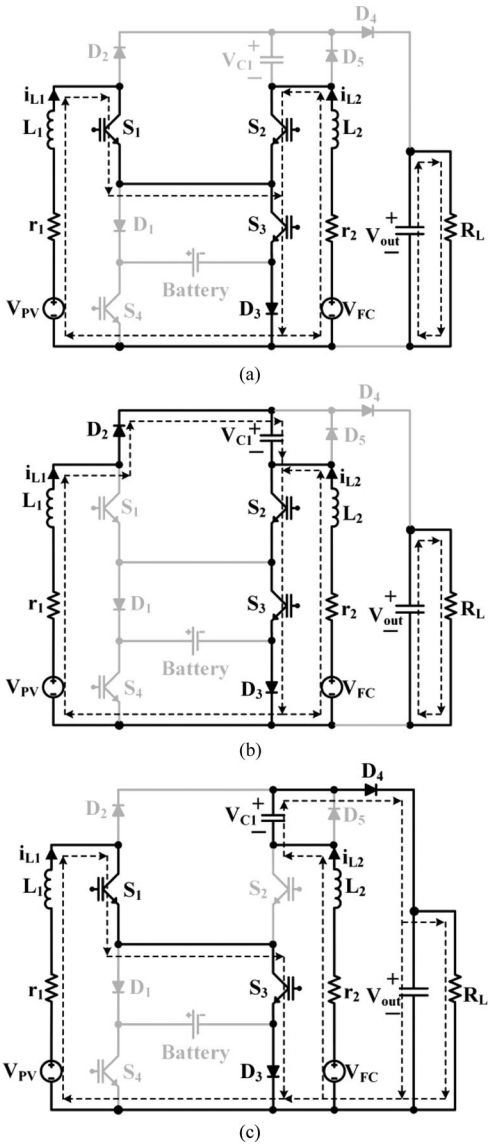

Fig. 3. Current-flow path of operating modes in first operating state. (a) Mode 1. (b) Mode 2. (c) Mode 3.

Also, by applying the current–second balance low over the capacitors C_1 and C_o, voltage of capacitor C_1, we have

$$C_1 : \ (d_2 - d_1)\, i_{L_1} - (1 - d_2)\, i_{L_2} = 0 \tag{5}$$

$$C_o : \ (1 - d_2)\, i_{L_2} = \frac{V_o}{R_{\text{Load}}}. \tag{6}$$

In this case, battery is not used and so we have

$$\begin{aligned} i_{\text{batt}} &= 0 \\ P_{\text{batt}} &= 0. \end{aligned} \tag{7}$$

B. Second Operation State (the Load is Supplied by PV, FC, and Battery)

In this state, as it is illustrated in Fig. 4, there are four operation modes. During this state, the load is supplied by all input sources (PV, FC, and battery). In first mode, there is only one current path. However, in other three modes, there are two current paths (through S_3 and D_3 or D_1 and S_4). In this state, current flows through D_1 and S_4. Switch S_4 is permanently ON during this state.

Mode 1: $(0 < t < d_1 T)$*:* In this interval, $S_1,\ S_2,\ S_3$, and S_4 are turned ON. Inductors L_1 and L_2 are charged by $V_{\text{PV}} + v_{\text{Battery}}$ and $V_{FC} + v_{\text{Battery}}$, respectively [see Fig. 4(a)].

Mode 2: $(d_1 T < t < d_2 T)$*:* In this interval, $S_1,\ S_2,\ S_4$, and D_1 are turned ON. Inductors L_1 and L_2 are charged by V_{PV} and V_{FC}, respectively [see Fig. 4(b)].

Mode 3: $(d_2\, T < t < d_3 T)$*:* In this interval, $S_2,\ S_4, D_1$, and D_2 are turned ON. Inductor L_1 is discharged to capacitor C_1 and L_2 is charged by v_{FC}[see Fig. 4(c)].

Mode 4: $(d_3 T < t < d_4 T)$*:* In this interval, $S_1,\ S_4, D_1$, and D_4 are turned ON. Inductor L_1 is charged by V_{PV} and inductor L_2 discharges C_1 to the output capacitor [see Fig. 4(d)].

By applying the voltage–second balance low over the inductors L_1 and L_2, we have

$$\begin{aligned} L_1 : d_1 \left[V_{\text{PV}} + V_{\text{batt}} - r_1 i_{L_1}\right] + (d_2 - d_1)\left[V_{\text{PV}} - r_1 i_{L_1}\right] \\ + (d_3 - d_2)\left[V_{\text{PV}} - r_1 i_{L_1} - V_{C_1}\right] + (1 - d_3)\left[V_{\text{PV}} - r_1 i_{L_1}\right] = 0 \end{aligned} \tag{8}$$

And then

$$V_{C_1} = \frac{V_{\text{PV}} + d_1 V_{\text{batt}} - r_1 i_{L_1}}{d_3 - d_2} \tag{9}$$

$$\begin{aligned} \times L_2 : d_1 \left[V_{FC} + V_{\text{batt}} - r_2 i_{L_2}\right] + (d_3 - d_1)\left[V_{FC} - r_2 i_{L_2}\right] \\ + (1 - d_3)\left[V_{FC} + V_{C_1} - r_2 i_{L_2} - V_o\right] = 0. \end{aligned} \tag{10}$$

And then

$$V_o = \frac{(d_3 - d_2)\left(V_{FC} + d_1 V_{\text{batt}} - r_2 i_{L_2}\right) + (1 - d_3)\left(V_{\text{PV}} + d_1 V_{\text{batt}} - r_1 i_{L_1}\right)}{(1 - d_3)(d_3 - d_2)}. \tag{11}$$

Also, by applying the current–second balance low over the capacitors C_1 and C_o, voltage of capacitor C_1, we have

$$C_1 : \ (d_3 - d_2)\, i_{L_1} - (1 - d_3)\, i_{L_2} = 0 \tag{12}$$

$$C_o : \ (1 - d_3)\, i_{L_2} = \frac{V_o}{R_{\text{Load}}}. \tag{13}$$

In this state, the current and power of battery can be calculated as (14) and (15), respectively

$$i_{\text{batt}} = d_1 \left(i_{L_2} + i_{L_1}\right) \tag{14}$$

$$P_{\text{batt}} = V_{\text{batt}} \left[d_1 \left(i_{L_2} + i_{L_1}\right)\right]. \tag{15}$$

C. Third Operation State (the Load is Supplied by PV and FC While Battery is in Charging Mode)

In this state, as it is illustrated in Fig. 5, there are four modes. During this state, PV and FC charges the battery and supply the energy of load. In the first- and second-operation modes, there

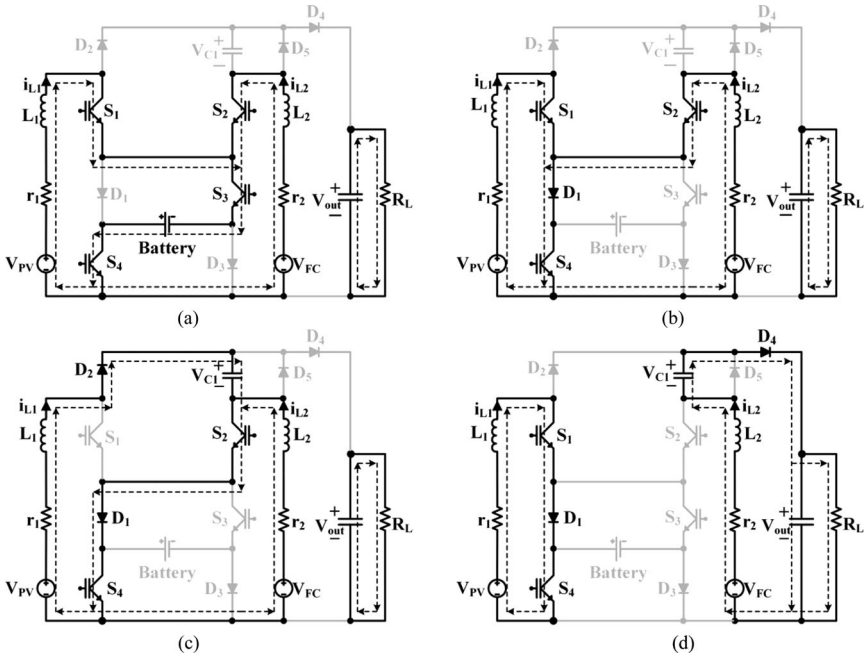

Fig. 4. Current-flow paths in different operation modes of second state. (a) Mode 1. (b) Mode 2. (c) Mode 3. (d) Mode 4.

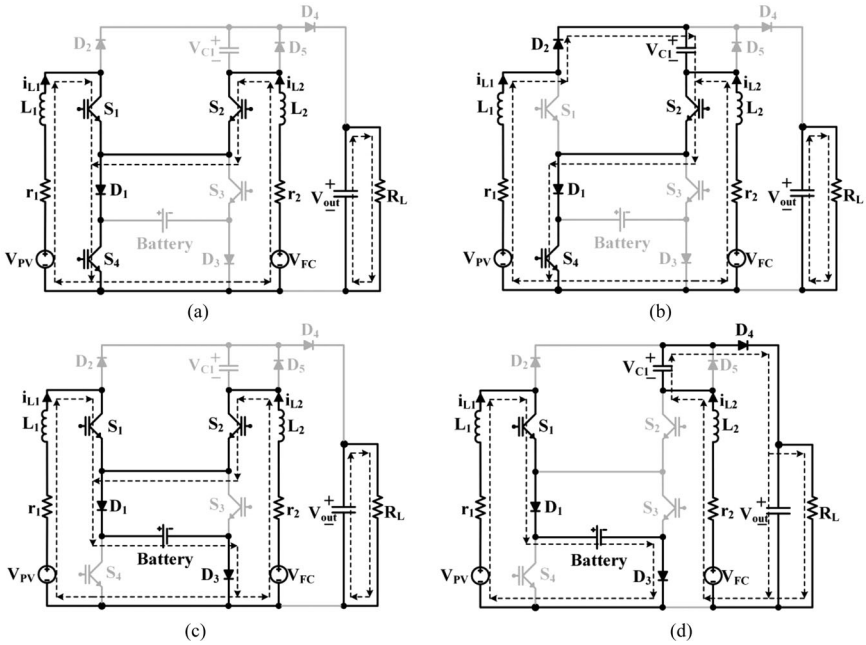

Fig. 5. Current-flow path of operating modes in third operating state. (a) Mode 1. (b) Mode 2. (c) Mode 3. (d) Mode 4.

are two possible current paths through S_3 and D_3 or D_1 and S_4). The path D_1 and S_4 is chosen to flow the current in this state. During this state, switch S_3 is permanently OFF and diode D_1 conducts.

Mode 1: $(0 < t < d_1 T)$*:* In this interval, S_1, S_2, S_4, and D_1 are turned ON. Inductors L_1 and L_2 are charged by v_{PV} and v_{FC}, respectively [see Fig. 5(a)].

Mode 2: $(d_1 T < t < d_2 T)$*:* In this interval, S_2, S_4, and D_1 are turned ON. Inductor L_1 is discharged to capacitor C_1 and inductor L_2 is charged by v_{FC} [see Fig. 5(b)].

Mode 3: $(d_2\, T < t < d_3\, T)$*:* In this interval, S_1, S_2, D_1, and D_3 are turned ON. Inductors L_1 and L_2 are charged by $v_{\mathrm{PV}} - v_{\mathrm{Battery}}$ and $v_{FC} - v_{\mathrm{Battery},}$ respectively [see Fig. 5(c)].

Mode 4: ($d_3\,T < t < d_4\,T$)*:* In this interval, $S_1,\ S_4, D_1$, and D_4 are turned ON. Inductor L_1 is charged by $v_{\rm PV} - v_{\rm Battery}$ and inductor L_2 is discharged by $v_{FC} - v_{C1} - v_o$[see Fig. 5(d)].

By applying the voltage–second balance low over the inductors L_1 and L_2, we have

$$L_1 : d_1\left[V_{\rm PV} - r_1 i_{L_1}\right] + (d_2 - d_1)\left[V_{\rm PV} - r_1 i_{L_1} - V_{C_1}\right] + (1 - d_2)\left[V_{\rm PV} - r_1 i_{L_1} - V_{\rm batt}\right] = 0 \tag{16}$$

$$V_{C_1} = \frac{V_{\rm PV} - (1 - d_2)\,V_{\rm batt} - r_1 i_{L_1}}{d_2 - d_1} \tag{17}$$

$$L_2 : d_2\left[V_{FC} - r_2 i_{L_2}\right] + (d_3 - d_2)\left[V_{FC} - r_2 i_{L_2} - V_{\rm batt}\right] + (1 - d_3)\left[V_{FC} + V_{C_1} - r_2 i_{L_2} - V_o\right] = 0 \tag{18}$$

$$V_o = \frac{(V_{FC} - (d_3 - d_2)\,V_{\rm batt} - r_2 i_{L_2})}{(1 - d_3)} + \frac{(V_{\rm PV} - (1 - d_2)\,V_{\rm batt} - r_1 i_{L_1})}{(d_2 - d_1)}. \tag{19}$$

By applying current–second balance low to capacitors C_1 and $C_{\rm o}$, we have

$$C_1 :\ (d_2 - d_1)\,i_{L_1} - (1 - d_3)\,i_{L_2} = 0 \tag{20}$$

$$C_o :\ (1 - d_3)\,i_{L_2} = \frac{V_o}{R_{\rm Load}}. \tag{21}$$

In this state, the current and delivered power by battery can be obtained as (22) and (23)

$$i_{\rm batt} = (d_3 - d_2)\,(i_{L_2} + i_{L_1}) + (1 - d_3)\,i_{L_1} \tag{22}$$

$$P_{\rm batt} = V_{\rm batt}\left[(d_3 - d_2)\,(i_{L_2} + i_{L_1}) + (1 - d_3)\,i_{L_1}\right]. \tag{23}$$

Fig. 6 illustrates switching pattern for each state and each mode. To fulfill switching operation, a saw-tooth wave as a carrier is compared with signals $d_1,\ d_2, d_3$, and d_4, which can independently control on state of power switches. Without considering output voltage utilized power of each sources PV, FC, and battery can be controlled using $d_1,\ d_2, d_3$, and d_4 signals. The voltage gain of the proposed converter is compared with the converter proposed in [24] in fig. 7.

As shown in this figure, the voltage gain of the proposed converter is higher than the converter proposed in [24]. Benefiting from high-voltage gain, the proposed converter achieve the specific output voltage V_O with less duty cycles in comparison with the converter proposed in [24] which increase the efficiency of the proposed converter.

It is worth noting that in this figure, the inductor resistances are ignored and the voltage gain is compared in the first operation mode. Input voltages are also considered the same.

IV. Dynamic Modeling and Control

In order to control and analyze dynamic performance of the proposed converter, it should be modeled. As it has been mentioned, the presented converter operates in three states that first state is made of three modes and second and third states are contained of four modes. Each state operates to provide particular goals, which will be explained. In first state, output voltage and only one of the input power sources can be controlled. Due to this fact in this paper, we decide to control PV power source, which can be replaced by FC source as well. In second state because of interference the battery, output voltages and input sources power rate can be controlled. Third states' control parameters due to interference the battery is same as second state.

As mentioned previously interference the battery consists of two states, which in one of them battery will be charged and in one of them battery will be discharged. Selection of proper state (without battery, battery charging, battery discharging) is depends on power managing algorithm. Dynamic model of the proposed converter for each state is as follows.

First state: In this state, d_1 and d_2 as control variables, control output voltage, and power rate of one of the input sources that is consider PV in this paper. State-space model of converter for first state is

$$L_1\frac{di_{L1}}{dt} = V_{\rm PV} + (d_1 - d_2)\,V_{C1} - r_1 i_{L1} \tag{24}$$

$$L_2\frac{di_{L2}}{dt} = V_{FC} + (1 - d_2)\,V_{C1} + (d_2 - 1)\,V_o - r_2 i_{L2} \tag{25}$$

$$C_o\frac{dV_o}{dt} = (1 - d_2)\,i_{L_2} - \frac{V_o}{R_{\rm Load}} \tag{26}$$

$$C_1\frac{dV_{C1}}{dt} = (d_2 - d_1)\,i_{L1} - (1 - d_2)\,i_{L2}. \tag{27}$$

Second state: In this state, three control variables $d_1,\ d_2$, and d_3 are used for controlling three state variables. In this state, the state-space model of converter is

$$L_1\frac{di_{L1}}{dt} = V_{\rm PV} + d_1 V_{\rm batt} + (d_2 - d_3)\,V_{C1} - r_1 i_{L1} \tag{28}$$

$$L_2\frac{di_{L2}}{dt} = V_{FC} + d_1 V_{\rm batt} + (1 - d_3)\,V_{C1} + (d_3 - 1)\,V_o - r_2 i_{L2} \tag{29}$$

$$C_o\frac{dV_o}{dt} = (1 - d_3)\,i_{L_2} - \frac{V_o}{R_{\rm Load}} \tag{30}$$

$$C_1\frac{dV_{C1}}{dt} = (d_3 - d_2)\,i_{L1} - (1 - d_3)\,i_{L2}. \tag{31}$$

Third state: In this state, same as second state, three state variables are controlled by three control variables $d_1,\ d_2$, and d_3 controlling. State-space model of the converter in this state can be written as follows:

$$L_1\frac{di_{L1}}{dt} = V_{\rm PV} + (d_2 - 1)\,V_{\rm batt} + (d_1 - d_2)\,V_{C1} - r_1 i_{L1} \tag{32}$$

$$L_2\frac{di_{L2}}{dt} = V_{FC} + (d_2 - d_3)\,V_{\rm batt} + (1 - d_3)\,V_{C1} + (d_3 - 1)\,V_o - r_2 i_{L2} \tag{33}$$

$$C_o\frac{dV_o}{dt} = (1 - d_3)\,i_{L_2} - \frac{V_o}{R_{\rm Load}} \tag{34}$$

$$C_1\frac{dV_{C1}}{dt} = (d_2 - d_1)\,i_{L1} - (1 - d_3)\,i_{L2}. \tag{35}$$

Assuming the small-signal method [25], input voltage, state variables, and duty ratios consist of two parts: steady values

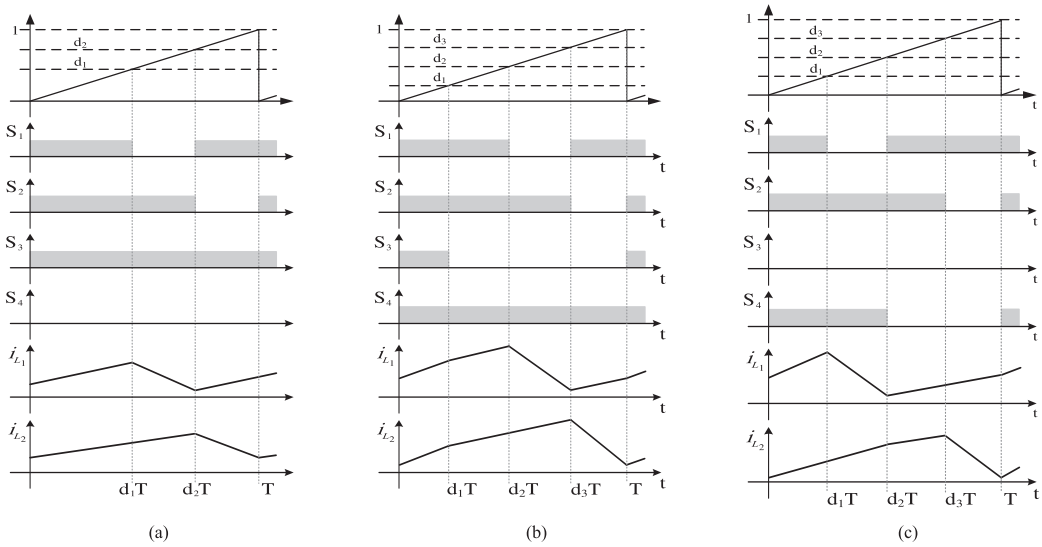

Fig. 6. Switching pattern for three states. (a) First state. (b) Second state. (c) Third state.

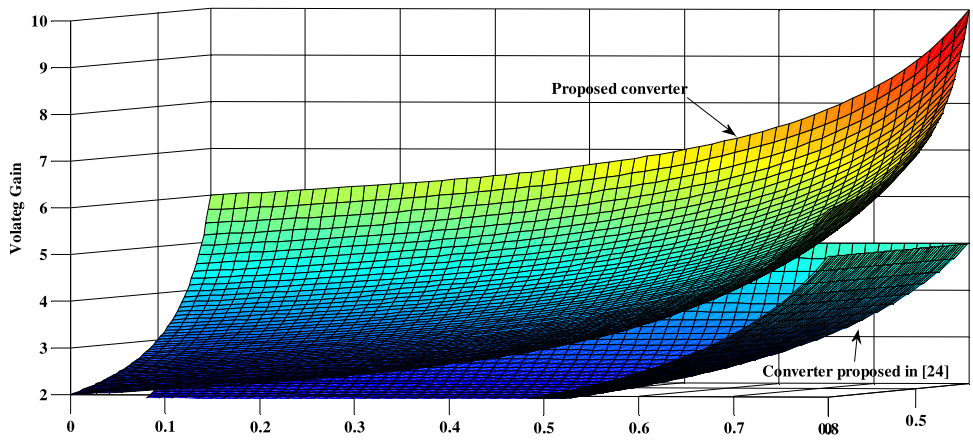

Fig. 7. Output voltage of the proposed converter and converter proposed in [24].

$(\bar{V}, \bar{X}, \bar{D})$ and perturbations $(\tilde{v}, \tilde{x}, \tilde{d})$ that are

$$v = \bar{V} + \tilde{v},\ x = \bar{X} + \tilde{x},\ d = \bar{D} + \tilde{d}. \tag{36}$$

Perturbations are assumed not to oscillate impressively in switching period ($\tilde{v} \ll \bar{V}, \tilde{x} \ll \bar{X}, \tilde{d} \ll \bar{D}$). Substituting (36) in (24)–(35) and neglecting the second-order terms result in a small-signal model. Small-signal models are shown in matrix form as

$$\begin{cases} \dot{\tilde{x}} = A\tilde{x} + B\tilde{u} \\ \tilde{y} = C\tilde{x} + D\tilde{u} \end{cases} \tag{37}$$

$\tilde{x},\ \tilde{u}$ and $\tilde{y}$ are state variable vector, control variables vector, and system output vector, respectively. Small-signal model for each state are

First state

$$A = \begin{bmatrix} -r_1 & 0 & 0 & \bar{d}_1 - \bar{d}_2 \\ 0 & -r_2 & \bar{d}_2 - 1 & 1 - \bar{d}_2 \\ 0 & 1 - \bar{d}_2 & -\dfrac{1}{R_{\text{Load}}} & 0 \\ \bar{d}_2 - \bar{d}_1 & \bar{d}_2 - 1 & 0 & 0 \end{bmatrix},$$

$$B = \begin{bmatrix} \bar{V}_{C1} & -\bar{V}_{C1} \\ 0 & \bar{V}_o - \bar{V}_{C1} \\ 0 & -\bar{i}_{L2} \\ -\bar{i}_{L1} & \bar{i}_{L1} + \bar{i}_{L2} \end{bmatrix}$$

$$C = \begin{bmatrix} 1 & 0 & 0 & 0 \\ 0 & 0 & 0 & 0 \\ 0 & 0 & 1 & 0 \\ 0 & 0 & 0 & 0 \end{bmatrix}, \tilde{x} = \begin{bmatrix} \tilde{i}_{L1} \\ \tilde{i}_{L2} \\ \tilde{V}_o \\ \tilde{V}_{C1} \end{bmatrix}, \tilde{u} = \begin{bmatrix} \tilde{d}_1 \\ \tilde{d}_2 \end{bmatrix}. \tag{38}$$

Second state

$$A=\begin{bmatrix} -r_1 & 0 & 0 & \bar{d}_2-\bar{d}_3 \\ 0 & -r_2 & \bar{d}_3-1 & 1-\bar{d}_3 \\ 0 & 1-\bar{d}_3 & -\dfrac{1}{R_{\rm Load}} & 0 \\ \bar{d}_3-\bar{d}_2 & \bar{d}_3-1 & 0 & 0 \end{bmatrix}, \tilde{u}=\begin{bmatrix} \tilde{d}_1 \\ \tilde{d}_2 \\ \tilde{d}_3 \end{bmatrix}$$

$$B=\begin{bmatrix} \bar{V}_{C1} & \bar{V}_{\rm batt} & 0 \\ 0 & \bar{V}_{\rm batt} & \bar{V}_o-\bar{V}_{C1}-\bar{V}_{\rm batt} \\ 0 & 0 & -\bar{i}_{L2} \\ -\bar{i}_{L1} & \bar{i}_{L1} & \bar{i}_{L2} \end{bmatrix},$$

$$C=\begin{bmatrix} 1 & 0 & 0 & 0 \\ 0 & 1 & 0 & 0 \\ 0 & 0 & 1 & 0 \\ 0 & 0 & 0 & 0 \end{bmatrix}, \tilde{x}=\begin{bmatrix} \tilde{i}_{L1} \\ \tilde{i}_{L2} \\ \tilde{V}_o \\ \tilde{V}_{C1} \end{bmatrix} \quad (39)$$

Third state

$$A=\begin{bmatrix} -r_1 & 0 & 0 & \bar{d}_1-\bar{d}_2 \\ 0 & -r_2 & \bar{d}_3-1 & 1-\bar{d}_3 \\ 0 & 1-\bar{d}_3 & -\dfrac{1}{R_{\rm Load}} & 0 \\ \bar{d}_2-\bar{d}_1 & \bar{d}_3-1 & 0 & 0 \end{bmatrix},$$

$$B=\begin{bmatrix} \bar{V}_{\rm batt} & \bar{V}_{C1} & -\bar{V}_{C1} \\ \bar{V}_{\rm batt} & 0 & \bar{V}_o-\bar{V}_{C1} \\ 0 & 0 & -\bar{i}_{L2} \\ 0 & -\bar{i}_{L1} & \bar{i}_{L1}+\bar{i}_{L2} \end{bmatrix}$$

$$C=\begin{bmatrix} 1 & 0 & 0 & 0 \\ 0 & 1 & 0 & 0 \\ 0 & 0 & 1 & 0 \\ 0 & 0 & 0 & 0 \end{bmatrix}, \tilde{x}=\begin{bmatrix} \tilde{i}_{L1} \\ \tilde{i}_{L2} \\ \tilde{V}_o \\ \tilde{V}_{C1} \end{bmatrix}, \tilde{u}=\begin{bmatrix} \tilde{d}_1 \\ \tilde{d}_2 \\ \tilde{d}_3 \end{bmatrix}. \quad (40)$$

Respect to the small-signal models of the proposed converter, the transfer function matrix can be obtained as follows:

$$G=C(SI-A)^{-1}B+D. \quad (41)$$

As mentioned, the first state comprises two control variables as well second and third states consist of three control variables. Due to aforementioned facts, the rank of the transfer function matrix represents the number of control variables, then for first state G_{2x2} and for second and third states G_{3x3} that are shown as

$$\underbrace{\begin{bmatrix} y_1 \\ y_2 \end{bmatrix}}_{y} = \underbrace{\begin{bmatrix} g_{11} & g_{12} \\ g_{21} & g_{22} \end{bmatrix}}_{G_{2\times 2}} \underbrace{\begin{bmatrix} u_1 \\ u_2 \end{bmatrix}}_{u} \quad (42)$$

$$\underbrace{\begin{bmatrix} y_1 \\ y_2 \\ y_3 \end{bmatrix}}_{y} = \underbrace{\begin{bmatrix} g_{11} & g_{12} & g_{13} \\ g_{21} & g_{22} & g_{23} \\ g_{31} & g_{32} & g_{33} \end{bmatrix}}_{G_{3\times 3}} \underbrace{\begin{bmatrix} u_1 \\ u_2 \\ u_3 \end{bmatrix}}_{u} \quad (43)$$

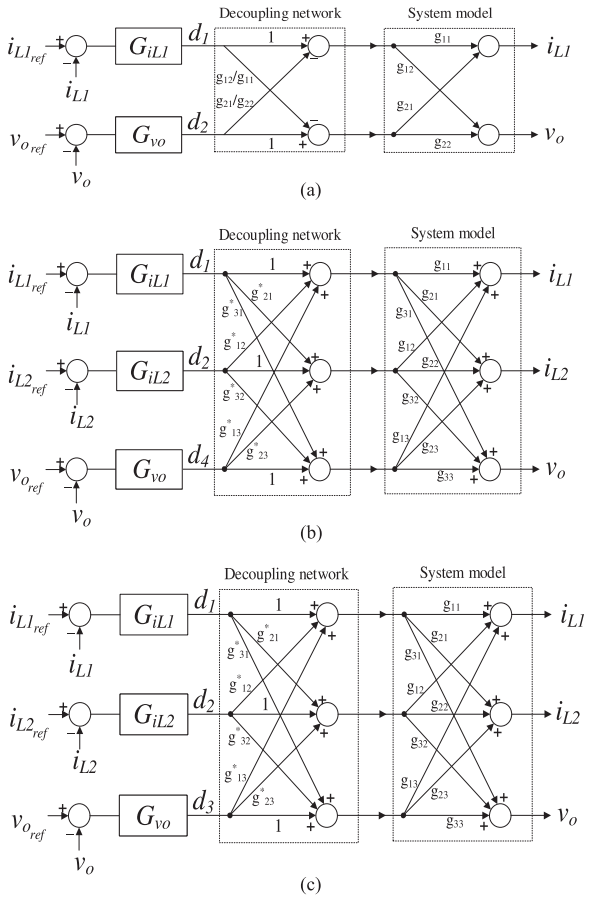

Fig. 8. Decoupling network for three states. (a) First state. (b) Second state. (b) Third state.

where y and u are the output and input vectors, respectively, and g_{ij} is the transfer function between y_i and u_j. In order to control the proposed converter's desired state variables independently, decoupling the transfer function is needed [24]. Fig. 8 represent decoupling network for three operation states. Considering Decoupling Network G^* [24], [25] and $x=Gu^*$ that u^* is the modified input consist of duty ratios $u^*=G^*u$. As a result, $x=GG^*u$. Base on the modern control theory [2], to provide each output of the matrixes be determined by each singular input, the matrix should be in diagonal arrange. Decoupling matrix $G^*=G^{-1}xu^{-1}$ for two controls and three control variables are

$$G^*_{2\times 2}=\begin{bmatrix} 1 & -\dfrac{g_{12}}{g_{11}} \\ -\dfrac{g_{21}}{g_{22}} & 1 \end{bmatrix} \quad (44)$$

$$G_{3\times 3}{}^*=\begin{bmatrix} 1 & \dfrac{g_{13}\cdot g_{32}-g_{12}\cdot g_{33}}{g_{11}\cdot g_{33}-g_{13}\cdot g_{31}} & \dfrac{g_{12}\cdot g_{23}-g_{13}\cdot g_{22}}{g_{11}\cdot g_{22}-g_{12}\cdot g_{21}} \\ \dfrac{g_{23}\cdot g_{31}-g_{21}\cdot g_{33}}{g_{22}\cdot g_{33}-g_{23}\cdot g_{32}} & 1 & \dfrac{g_{13}\cdot g_{21}-g_{11}\cdot g_{23}}{g_{11}\cdot g_{22}-g_{12}\cdot g_{21}} \\ \dfrac{g_{21}\cdot g_{32}-g_{22}\cdot g_{31}}{g_{22}\cdot g_{33}-g_{23}\cdot g_{32}} & \dfrac{g_{12}\cdot g_{31}-g_{11}\cdot g_{32}}{g_{11}\cdot g_{33}-g_{13}\cdot g_{31}} & 1 \end{bmatrix} \quad (45)$$

TABLE I
CONTROLLER PARAMETERS

	GV_o	GI_{L1}	GI_{L2}
STATE I	$K_p = 0.5466$	$K_p = 7.0000$	$K_p = -$
	$K_I = 48.3721$	$K_I = 3.1439$	$K_I = -$
STATE II	$K_p = 0.4983$	$K_p = -0.0811$	$K_p = 0.3303$
	$K_I = 65.7330$	$K_I = -9.7503$	$K_I = -7.6737$
STATE III	$K_p = 0.2983$	$K_p = 0.0001$	$K_p = 0.4303$
	$K_I = 65.7330$	$K_I = 0.0150$	$K_I = -8.0737$

Employing decoupling matrixes (44) and (45) result in independent single-loop control for each input in both two and three control variables which for two control variables state are

$$\frac{y_1}{u_1} = g_{11} - g_{12}\frac{g_{21}}{g_{22}}$$
$$\frac{y_2}{u_2} = -g_{12}\frac{g_{21}}{g_{11}} + g_{22}. \quad (46)$$

And for three control variables states are

$$\frac{y_1}{u_1} = g_{11} + g_{12}\frac{g_{13}\cdot g_{32} - g_{12}\cdot g_{33}}{g_{11}\cdot g_{33} - g_{13}\cdot g_{31}} + g_{13}\frac{g_{12}\cdot g_{23} - g_{13}\cdot g_{22}}{g_{11}\cdot g_{22} - g_{12}\cdot g_{21}}$$
$$\frac{y_2}{u_2} = g_{21}\frac{g_{23}\cdot g_{31} - g_{21}\cdot g_{33}}{g_{22}\cdot g_{33} - g_{23}\cdot g_{32}} + g_{22} + g_{23}\frac{g_{13}\cdot g_{21} - g_{11}\cdot g_{23}}{g_{11}\cdot g_{22} - g_{12}\cdot g_{21}}$$
$$\frac{y_3}{u_3} = g_{31}\frac{g_{21}\cdot g_{32} - g_{22}\cdot g_{31}}{g_{22}\cdot g_{33} - g_{23}\cdot g_{32}} + g_{32}\frac{g_{12}\cdot g_{31} - g_{11}\cdot g_{32}}{g_{11}\cdot g_{33} - g_{13}\cdot g_{31}} + g_{33}. \quad (47)$$

In order to control the decoupled transfer functions proportional-integral (PI) controller is used to remove steady-state errors of the system. To reach desire phase margin $60^\circ \leq \mathrm{P.M} \leq 80^\circ$ and proper gain margin $\mathrm{G.M} \geq 10\mathrm{db}$ with suitable cutoff frequency. A PI controller is designed as $K_P + \frac{K_I}{S}$ [24]. The PI controller's parameters for each state are shown in Table I regard to mentioned conditions. Bode plot of frequency response of open-loop and closed-loop transfer functions of the converter are presented in Figs. 9–11.

As it can be seen from Figs. 9–11 with using proper designed PI controller, we can achieve to -20-db/dec slope in low frequencies and appropriate P.M which causes to gain stable system.

V. POWER MANAGEMENT AND MPPT ALGORITHM

The multipowered HEV has a construction as depicted in Fig. 1. In the drive system, the FC is the main power supply. Rooftop PV panel is employed to reduce the fuel consumption and charging the battery. The battery is utilized as storage device. With a proper design, there will be no need for an external electrical supply to charge the battery [26]. The battery can be charged via PV, FC. In order to have the system operated in optimum region, the following criteria have to be ensured:

1) electrical motor always supplies the demand power;
2) PV panel and FC operate in their optimal region;
3) the battery energy level should be always within the optimum region.

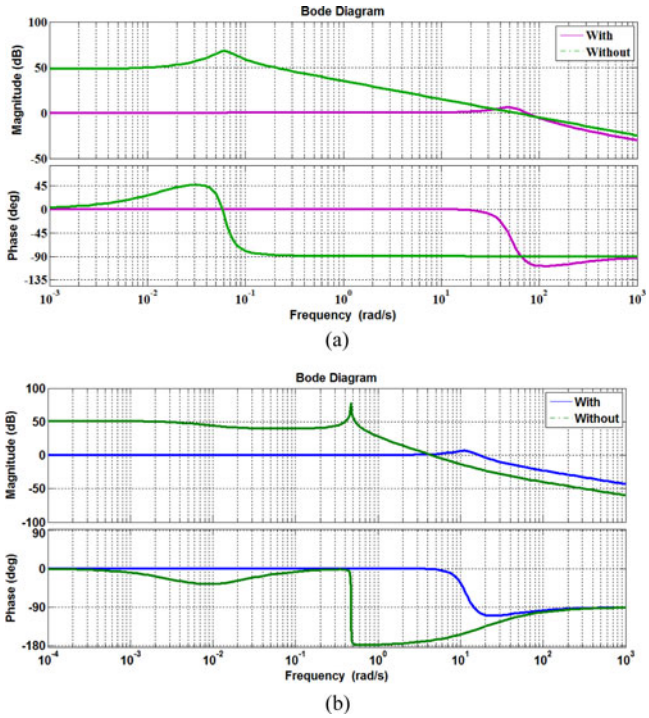

Fig. 9. Bode plot of first state. (a) Output voltage (V_o). (b) Input current (I_{L1}).

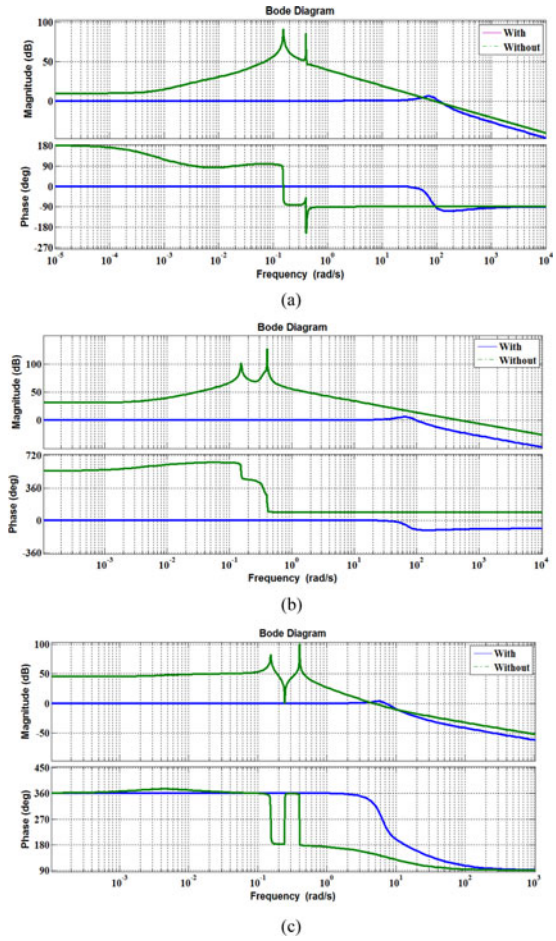

Fig. 10. Bode plot of second state. (a) Output voltage (V_o). (b) Input current of PV (I_{L1}). (c) Input current of FC (I_{L2}).

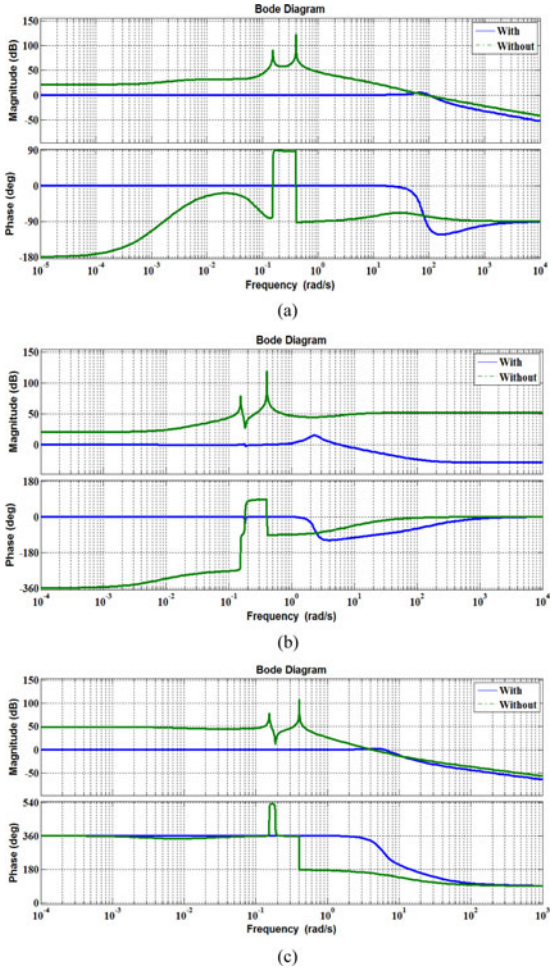

Fig. 11. Bode plot of third state. (a) Output voltage (V_o). (b) Input current of PV (I_{L1}). (c) Input current of FC (I_{L2}).

The power management procedure is described below and the flowchart of the strategy is depicted in Fig. 12.

1) Control signals, acceleration, and brake, identify the command power.
2) In case command power is less than maximum PV power and battery energy level is less than minimum energy level, PV will work at MPP and extra energy will be stored in battery. If command power is less than maximum PV power but battery energy level is more than minimum energy level, PV will generate the command power and the battery remains off. In both conditions, FC is off.
3) If command power is more than maximum PV power, PV panel will operate in MPP and new command power will be defined as

$$P_{\text{command}}^{\text{new}} = P_{\text{command}} - P_{\text{PV}}. \tag{48}$$

4) New command power is compared with FC's rated power. Given that the new command power is greater than rated power of FC, the FC will works at its rated power and battery will provide the rest of demanded power.

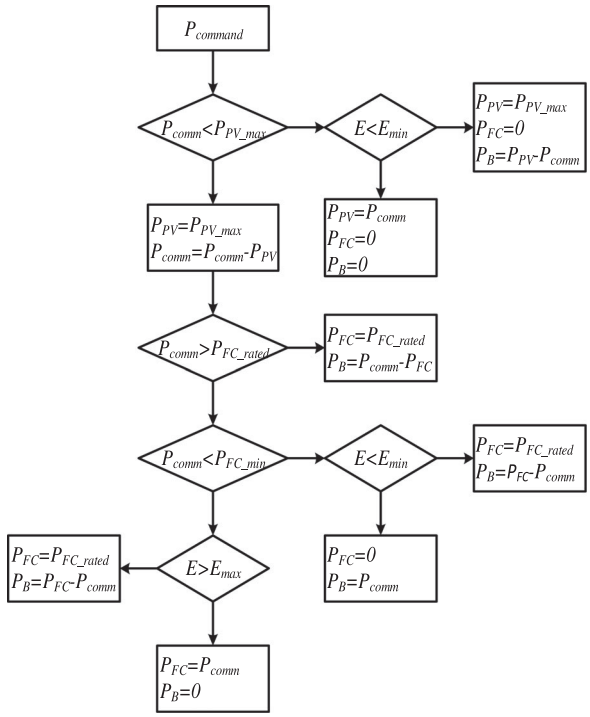

Fig. 12. Power managing strategy's flowchart.

VI. Additional Advantages of the Converter, Making It Suitable for HEVs

The proposed converter has the advantage of utilizing only one resource in case the other power sources cannot provide energy. This capability enhances the safety and reliability of the proposed converter. Different possible states are described as follows.

A) PV ON and FC OFF

Due to the long start-up time of the fuel cell, this state happens mostly at the starting the car or when the car is run out of fuel cell gas. In this state, battery can be charged or discharged by PV. Because of the facts that FC is the main power supply and ESS has a limited capacity, this state cannot be so long. In order to let the PV operate individually, switch S_2 is turned off and instead of capacitor C_1, the power of PV is transferred to the output capacitor C_o. According to the presented topology, battery can be charged and discharged via PV and by controlling switches S_1, S_3, and S_4.

B) PV OFF and FC ON

As mentioned above, FC is the main power source to provide the demanded power by HEV individually because the energy of PV is less than FC and depends on climate situation. Therefore, an extra diode (D_5) is paralleled with capacitor C_1. The diode D_5 is OFF when capacitor C_1 is charged. When the FC is utilized individually, the capacitor C_1 discharges until its voltage is zero. When the voltage across capacitor C_1 is going to be negative, diode D_5 will be turned on and clamps the voltage of capacitor C_1.

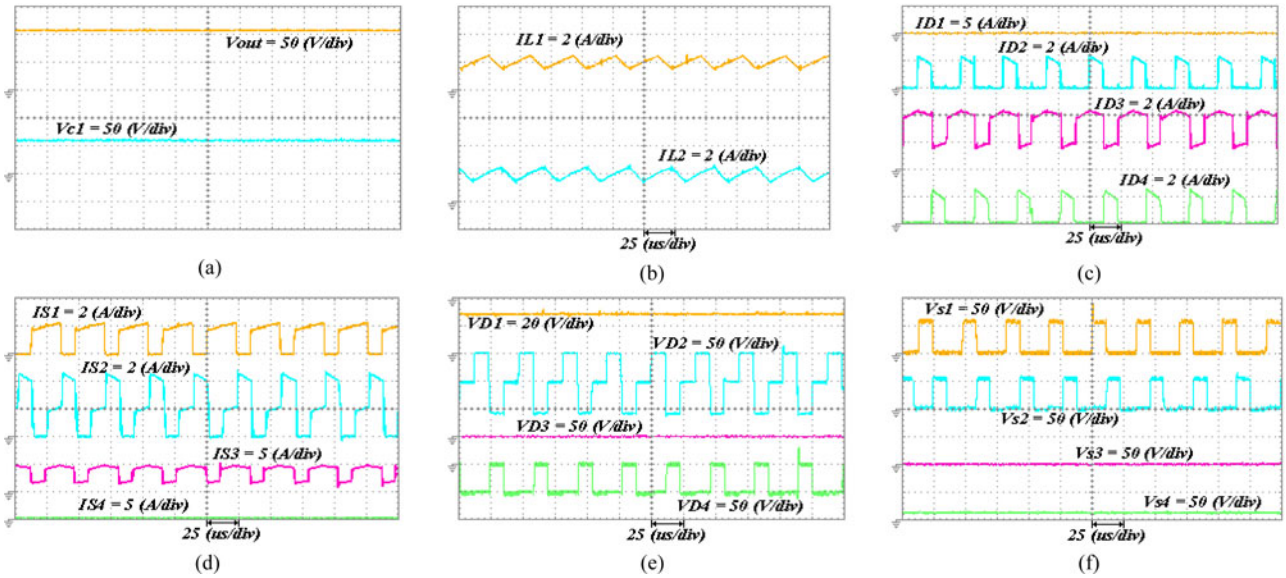

Fig. 13. Experimental results of the first operation state.

VII. Experimental Results

In order to verify the performance of the proposed converter, an 80-W prototype version of the circuit is built and tested in presented three states. Switching frequency is considered about 30 KHz. A digital signal processor (DSPIC30F4011) is employed to control power switches. As mentioned earlier, the proposed converter has the capability of being used for different industrial and domestic applications, such as HEV, DGs interface, smart homes. Power sources are mainly PV arrays, fuel cells, etc. Ignoring the transient time of the power sources, they could be replaced by dc power supplies to obtain experimental results. Both of the input sources are set on 20 V. A Li-ion 12-V 7-Ah battery is used as an energy storage element. Li-ion type batteries are used widely due to their excellent performance in portable electronic gadgets [27]. High reliability, high energy density, high-temperature performance, and being recyclable are main features of Li-ion batteries. However, their high cost is one of their drawbacks [27]. Due to high switching frequency, ferrite cores are chosen for the both inductors. The value of the inductor L_1 is $550(\mu\mathrm{H})$ and the inductor L_2 is $650\,\mu$H. Capacitors utilized in the converter are $470\,\mu$F. Fig 13 shows first states operation results. Fig 13(a) shows output and capacitor C_1's voltage. Considering 20 V for each input-source voltage properly boosted to about 110 V. Inductors current is shown in Fig. 13(b) and (c) and Fig. 13(d) represent diodes and power switches current. Diodes and power switches voltage is shown in Fig. 13(e) and (f). In the experimental results of first operation mode, the inductor currents are about 2 A. As shown in Fig. 13(c) and (d), the currents of diode D_1 and switch S_4 are zero while diode D_3 and switch S_3 are always on which cause the voltage across them to be about zero. The other components are being switched with the frequency of 30 kHz.

Second state's operation results are shows in Fig. 14. Fig. 14(a) shows the output and capacitor C_1's voltage. Inductors L_1 and L_2 current is illustrated in Fig. 14(b). Diodes and power switches' currents are shown in Fig. 14(c) and (d). Fig. 14(e) and (f) illustrates diodes' and power switches' voltage, respectively. Fig. 14(g) shows batteries current. In this operation mode, the inductor currents are about 2 A with a ripple of 1 A. Besides, the battery is discharged by the current of 3 A flows through it. In this operation mode, all switches are being switched and just diode D_3 is always OFF. This caused the efficiency of the converter in this mode to be less than the others.

Third state's experimental results are shown in Fig. 15. Voltage of capacitor C_1 and output voltage of the proposed converter is shown is Fig. 15(a). Fig. 15(b) illustrates inductors' currents. Current of diodes and power switches is shown in Fig. 15(c) and (d), respectively.

Fig. 15(e) and (f) illustrates voltage of diodes and power switches. Battery's current is also shown in Fig. 15(g). In this operation mode, the inductor currents are about 2 A too. The battery is charged in this mode. Despite discharging mode, the current flows through the battery has three amounts, 0, 5, and 2 A. Switch S_3 is OFF in this mode and the voltage across it is always equals to V_{Bat}.

Results validate the promising performance of the converter in each state. Fig. 16 shows the efficiency of the experimental results in three operation states. As shown in this figure, the proposed converter efficiency in first operation state is more than the others. The least efficiency of the proposed converter is about %85 which occur in discharging mode. Because the switches used in this mode are more than the others. Therefore, the switching loss in this mode is more than other modes.

In order to verify the performance of the control system following experiment is established, Fig. 17(a) and (b) shows the input sources and battery's current and output voltage.

In this experiment, in the first state, output desired voltage is considered to be about 120 V and PV desired current is about 2 A. As mentioned, in this state, battery's power is zero. In the second part of the experiment, PV's reference current increases

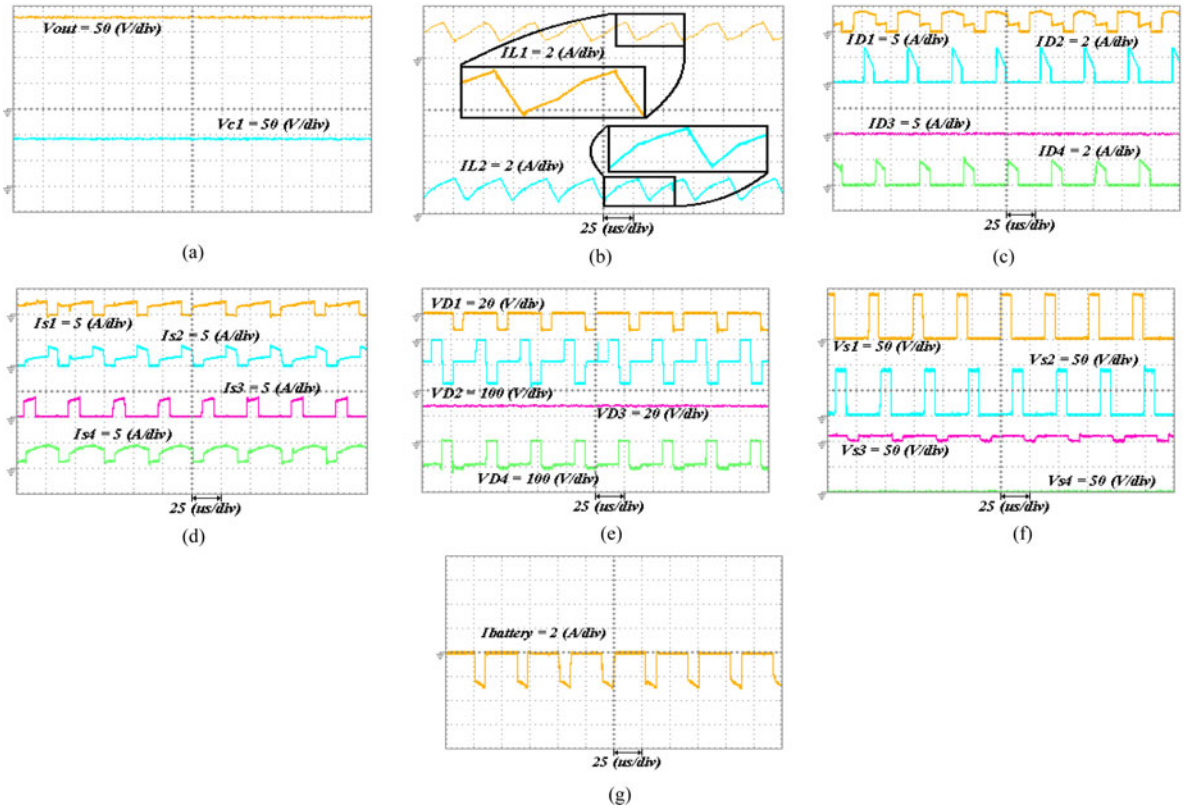

Fig. 14. Experimental results of the second operation state.

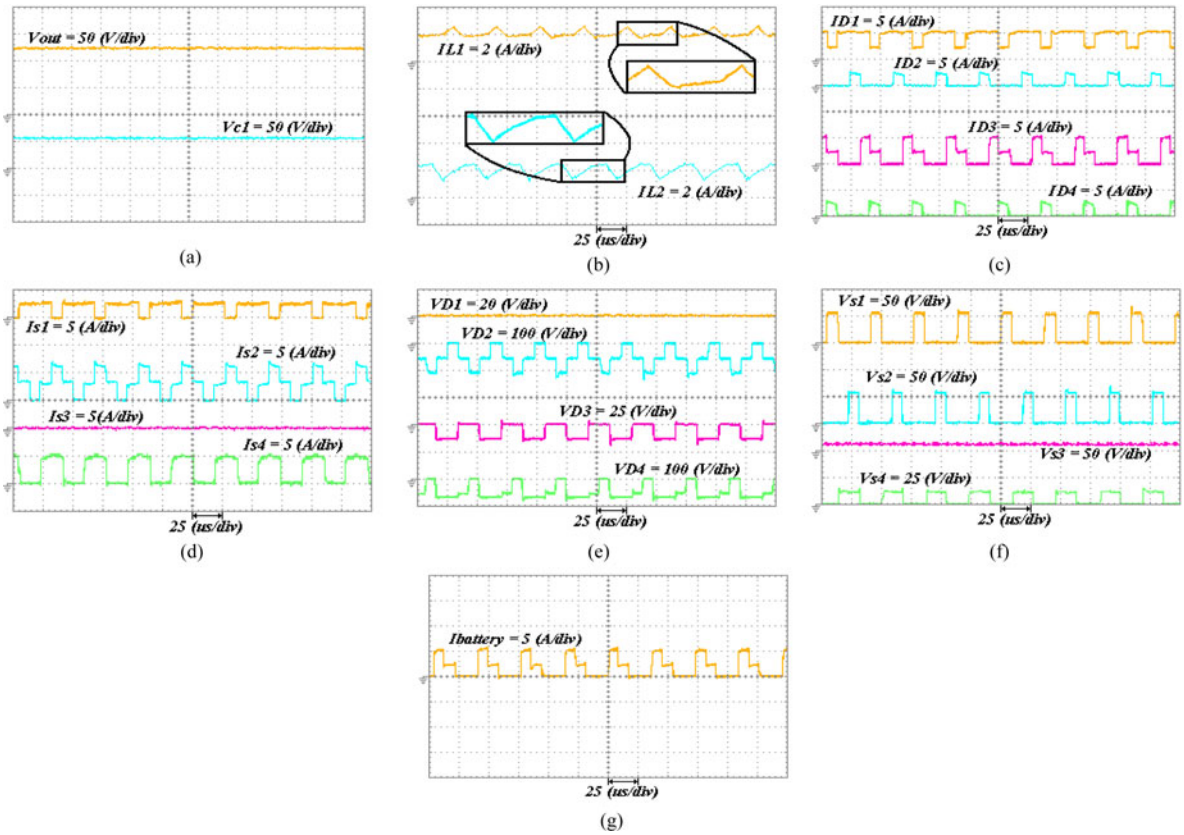

Fig. 15. Experimental results of the third operation state.

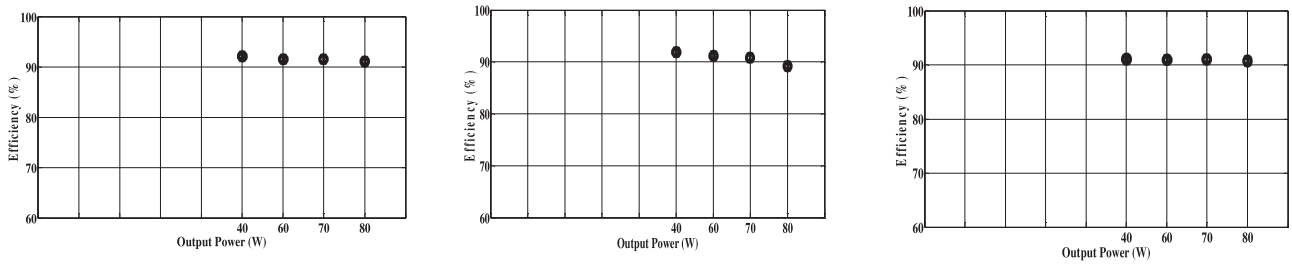

Fig. 16. Experimental efficiency of the proposed converter. (a) No Battery. (b) Battery discharging. (c) Battery charging.

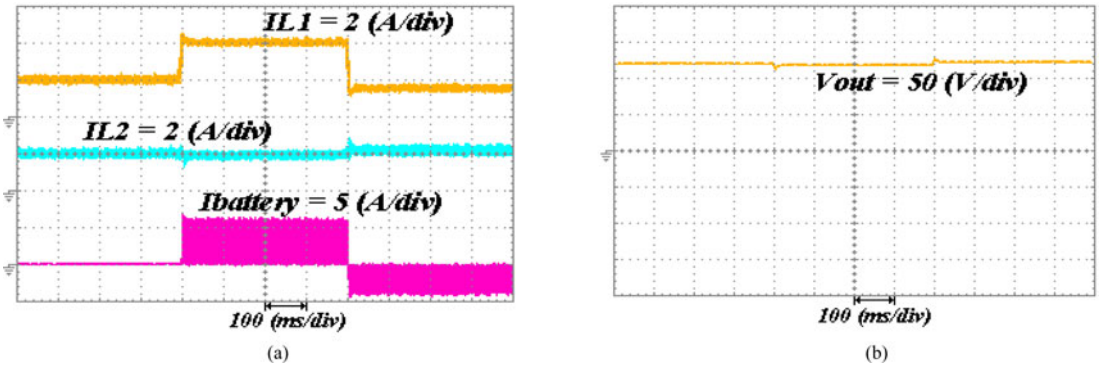

Fig. 17. Experimental performance of the proposed control system. (a) Inputs' and battery's current. (b) Output voltage.

to 4 A and FC's reference current is 2 A and output desired voltage is 120 V. The overshoot of the current of inductor L_1 is acceptable. The current of inductor L_2 is a bit less than its previous amount. The current flow through the battery is about 6 A. These reference values cause the circuit to operate in battery charging mode with 40 W.

Third part of the experiment establish with 1.7 A for PV and 2 A for FC and 120 V for output voltage that result in 7-W battery discharging. The current flow through the battery is about 4 A. The current of inductor is more than the previous amounts.

In these three stages, the output voltage is changes but it is ignorable. The transient response of the converter is acceptable and can be applied in HEV applications.

VIII. Conclusion

In this study, a novel three-input dc/dc converter is proposed and analyzed thoroughly. The converter has the capability of providing the demanded power by load in absence of one or two resources. The promising performance of the converter and employed control method offer a high reliability for utilizing the converter in industrial and domestic applications. The converter is modeled for three different operational states and utilized to design a proper controller. MPPT algorithm is achieved and along power management is utilized to apply the commands of controller. Meanwhile, employing power management and MPPT procedure will enhance the efficiency of the converter. Finally, a laboratory prototype of the presented converted is implemented and results are taken and depicted. Results prove the analysis and performance of the converter.

References

[1] A. Ostadi and M. Kazerani, "Optimal sizing of the battery unit in a plug-in electric vehicle," *IEEE Trans. Veh. Technol.*, vol. 63, no. 7, pp. 3077–3084, Sep. 2014.

[2] P. Mulhall, S. M. Lukic, S. G. Wirashingha, Y.-J. Lee, and A. Emadi, "Solar-assisted electric auto rickshaw three-wheeler," *IEEE Trans. Veh. Technol.*, vol. 59, no. 5, pp. 2298—2307, Jun. 2010.

[3] H. J. Chiu and L. W. Lin, "A bidirectional dc-dc converter for fuel cell electric vehicle driving system," *IEEE Trans. Power Electron.*, vol. 21, no. 4, pp. 950–958, Jul. 2006.

[4] T. Markel, M. Zolot, K. B. Wipke, and A. A. Pesaran, "Energy storage requirements for hybrid fuel cell vehicles," *presented at the Adv. Autom. Battery Conf.*, Nice, France, 2003.

[5] S. Miaosen, "Z-source inverter design, analysis, and its application in fuel cell vehicles," *Ph.D. dissertation*, Dept. Electr. Comput. Eng., Michigan State Univ., East Lansing, MI, USA, 2007.

[6] O. Hegazy, R. Barrero, J. Van Mierlo, P. Lataire, N. Omar, and T. Coosemans, "An advanced power electronics interface for electric vehicles applications," *IEEE Trans. Power Electron.*, vol. 28, no. 12, pp. 1–14, Dec. 2013.

[7] M. R. Feyzi, S. A. KH. Mozaffari Niapour, F. Nejabatkhah, S. Danyali, and A. Feizi, "Brushless DC motor drive based on multi-input DC boost converter supplemented hybrid PV/FC/Battery power system," in *Proc. IEEE Electr. Comput. Eng. Conf.*, 2011, pp. 000442–000446.

[8] R. J. Wai, C. Y. Lin, and B. H. Chen, "High-efficiency DC–DC converter with two input power sources," *IEEE Trans. Power Electron.*, vol. 27, no. 4, pp. 1862–1875, Apr. 2012.

[9] L. J. Chien, C. C. Chen, J. F. Chen, and Y. P. Hsieh, "Novel three-port converter with high-voltage gain," *IEEE Trans. Power Electron.*, vol. 29, no. 9, pp. 4693–4703, Sep. 2014.

[10] R. B. Mohammad, H. Ardi, R. Alizadeh, and A. Farakhor, "Non-isolated multi-input–single-output DC/DC converter for photovoltaic power generation systems," *IET Power Electron.*, vol. 7, no. 11, pp. 2806–2816, Jun. 2014.

[11] L. W. Zhou, B. X. Zhu, and Q. M. Luo, "High step-up converter with capacity of multiple input," *IET Power Electron.*, vol. 5, no. 5, pp. 524–531, May 2012.
[12] A. Ajami, H. Ardi, and A. Farakhor, "A novel high step-up DC/DC converter based on integrating coupled inductor and switched-capacitor techniques for renewable energy applications," *IEEE Trans. Power Electron.*, vol. 30, no. 8, pp. 4255–4263, Aug. 2015.
[13] H. Ardi, R. R. Ahrabi, and S. N. Ravandanegh, "Non-isolated bidirectional DC–DC converter analysis and implementation," *IET Power Electron.*, vol. 7, no. 12, pp. 3033–3044, Jun. 2014.
[14] R. Y. Duan and J. D. Lee, "High-efficiency bidirectional DC–DC converter with coupled inductor," *IET Power Electron.*, vol. 5, no. 1, pp. 115–123, Jun. 2012.
[15] S. Danyali, S. H. Hosseini, and G. B. Gharehpetian, "New extendable single-stage multi-input DC–DC/AC boost converter," *IEEE Trans. Power Electron.*, vol. 29, no. 2, pp. 775–788, Feb. 2014.
[16] L. Wang, Z. Wang, and H. Li, "Asymmetrical duty cycle control and decoupled power flow design of a three-port bidirectional DC-DC converter for fuel cell vehicle application," *IEEE Trans. Power Electron.*, vol. 27, no. 2, pp. 891–904. Feb. 2012.
[17] S. Falcones, R. Ayyanar, and X. Mao, "A DC–DC multiport-converter-based solid-state transformer integrating distributed generation and storage," *IEEE Trans. Power Electron.*, vol. 28, no. 5, pp. 2192—2203, May 2013.
[18] Y. M. Chen, A. Q. Huang, and X. Yu, "A high step-up three-port DC-DC converter for stand-alone PV/battery power systems," *IEEE Trans. Power Electron.*, vol. 28, no. 11, pp. 5049–5062, Nov. 2013.
[19] K. Gummi and M. Ferdowsi, "Double-input DC–DC power electronic converters for electric-drive vehicles—Topology exploration and synthesis using a single-pole triple-throw switch," *IEEE Trans. Ind. Electron.*, vol. 57, no. 2, pp. 617–623, Feb. 2010.
[20] R.-J. Wai, S.-J. Jhung, J.-J. Liaw, and Y.-R. Chang, "Intelligent optimal energy management system for hybrid power sources including fuel cell and battery," *IEEE Trans. Power Electron.*, vol. 28, no. 7, pp. 3231–3244, Jul. 2013.
[21] S. Kelouwani, N. Henao, K. Agbossou, Y. Dube, and L. Boulon, "Two layer energy-management architecture for a fuel cell HEV using road trip information," *IEEE Trans. Veh. Technol.*, vol. 61, no. 9, pp. 3851–3864, Nov. 2012.
[22] M. A. G. de Brito, L. Galotto, L. P. Sampaio, G. de Azevedo e Melo, and C. A. Canesin, "Evaluation of the main MPPT techniques for photovoltaic applications," *IEEE Trans. Ind. Electron.*, vol. 60, no. 3, pp. 1156–1167, Mar. 2013.
[23] M. Koot, J. Kessels, B. de Jager, W. Heemels, P. Van den Bosch, and M. Steinbuch, "Energy management strategies for vehicular electric power systems," *IEEE Trans. Veh. Technol.*, vol. 54, no. 3, pp. 771–782, May 2005.
[24] F. Nejabatkhah, S. Danyali, S. H. Hosseini, and M. Sabahi Niapour, "Modeling and control of a new three-input DC–DC boost converter for hybrid PV/FC/battery power system," *IEEE Trans. Power Electron.*, vol. 27, no. 5, pp. 2309–2324, May 2012.
[25] Z. Qian, O. A. Rahman, H. A. Atrash, and I. Batarseh, "Modeling and control of three-port DC/DC converter interface for satellite applications," *IEEE Trans. Power Electron.*, vol. 25, no. 3, pp. 637–649, Mar. 2010.
[26] M. Eshani, Y. Gao, S. E. Gay, and A. Emadi, *Modern Electric, Hybrid Electric, and Fuel Cell Vehicles-Fundamentals, Theory, and Design*. Boca Raton, FL, USA: CRC Press, 2004, pp. 459–470.
[27] A. Khaligh and Z. Li, "Battery, ultracapacitor, fuel cell, and hybrid energy storage systems for electric, hybrid electric, fuel cell, and plug-in hybrid electric vehicles: State of the art," *IEEE Trans. Veh. Technol.*, vol. 59, no. 6, pp. 2806–2814, Jul. 2010.

Rouzbeh Reza Ahrabi received the B.Sc. and M.Sc. degrees in power electronics from Azarbaijan Shahid Madani University, Tabriz, Iran, in 2012 and 2014, respectively.

He was Honor as second-class at the Electrical Engineering Faculty, Azarbaijan Shahid Madani University. His main research interests include power electronic converters, power management, and nonlinear control. He is currently focusing on the grid-connected interface converters.

Hossein Ardi was born in Miyaneh, Iran, in 1990. He received the B.Sc. degree in electrical engineering and the M.Sc.(first-class Hons.) degree in power electronic engineering from Azarbaijan Shahid Madani University, Tabriz, Iran, in 2012 and 2014, respectively, where he is currently working toward the Ph.D. degree in power electronic engineering at the Faculty of Engineering.

His research interests include renewable energies, power electronic converters, especially high-step-up dc–dc converters, and multiinput converters. He is currently focusing on the single-stage multiinput converters.

Dr. Ardi is a Member of Organization Exceptional Talents at the Azarbaijan Shahid Madani University. He was also selected as the best student researcher at Azarbaijan Shahid Madani Univertsity in 2015.

Mahdi Elmi received the B.Sc. and M.Sc. degrees in power electronics from Azarbaijan Shahid Madani University, Trabriz, Iran, in 2012 and 2014, respectively, where he is currently working toward the Ph.D. degree in electrical engineering.

His research interests include power electronic converters, passive and active filters, and wind turbines. He is currently working on high step-up multiinput converters.

Ali Ajami received the B.Sc. and M.Sc. degrees in electronic engineering and power engineering, and the Ph.D. degree in power engineering from the Electrical and Computer Engineering Faculty of Tabriz University, Tabriz, Iran, in 1996, 1999, and 2005, respectively.

He is currently the Professor at the Electrical Engineering Department, Azarbaijan Shahid Madani University, Tabriz. His main research interests include dynamic and steady-state modeling and analysis of FACTS devices, harmonics and power quality compensation systems, microprocessors, DSP and computer-based control systems, and applications of power electronics converters for renewable energy.